Hindawi
Geofluids
Volume 2022, Article ID 7582916, 23 pages
https://doi.org/10.1155/2022/7582916

Research Article

Grouting Treatment and Parameters Optimization in Watery Karst Areas of High Speed Railway Tunnel Based on Comprehensive Geological Forecast: A Case Study

Shan Wu,[1] **Weichao Qiu**,[2] **Dunwen Liu**,[1] **and Yu Tang**[1]

[1]*School of Resources and Safety Engineering, Central South University, Changsha 410083, China*
[2]*Road & Bridge North China Engineering CO., LTD., Beijing 101100, China*

Correspondence should be addressed to Yu Tang; tangyu12@csu.edu.cn

Received 10 June 2022; Revised 16 September 2022; Accepted 7 October 2022; Published 16 November 2022

Academic Editor: Jim Shiau

Copyright © 2022 Shan Wu et al. This is an open access article distributed under the Creative Commons Attribution License, which permits unrestricted use, distribution, and reproduction in any medium, provided the original work is properly cited.

Based on the failure of the initial grouting scheme in tunnel engineering, an integrated geological forecasting system incorporating an industrial endoscope was used to detect watery karst areas in this tunnel. Numerical simulations were used to analyze the change patterns of arch top settlement, arch bottom bulge, and water surge in the tunnel under different grouting thicknesses. Compared to the displacement of the support structure, curtain grouting thickness is mainly reflected in reducing the amount of water surge. When the grouting thickness exceeds 5 m, the water-stopping effect of the tunnel is almost unchanged. Finally, a grout thickness of 5 m and a grout length of 25 m were selected as the grouting range for this project. During grouting, the combination of the three grouting techniques can effectively solve the problems of high water surges and difficult hole formation. The principle of "combination of exploration and injection" was followed to obtain real-time geological information and optimize the subsequent grouting plan. After the grouting, the grouting evaluation results and the field construction conditions showed that the grouting effect was good.

1. Introduction

Karst landscapes are formed as a result of the dissolution of soluble rock—particularly limestone. They have a significant degree of unpredictability and heterogeneity, by which various hazards may be caused [1–4]. For example, 19 major water gushing disasters have occurred in the Malujing tunnel of the Yiwan railway, resulting in 15 deaths and construction delays of more than 2 years. During the construction of the Xuefengshan tunnel, 36 water inrush and 63 collapse disasters occurred, causing 26 tunnels boring machine (TBM) tunnel accidents over 15 years [5]. The complex geological conditions are a serious challenge for the prevention of water and mud surges and collapses. To prevent the surrounding rock deformation and sudden water and mud disasters in the tunnel, many measures have been taken.

On the one hand, detecting karst areas before excavation is important. In the past 50 years, advanced detection has evolved from nongeophysical methods to nondestructive geophysical methods. Tunnel seismic prediction (TSP) is a widely used system developed by Alimoradi et al. and Ismail et al. [6, 7]. Li et al. proposed the standard of using the TSP method to detect typical geological anomalies [8]. However, TSP is not sensitive to the watery areas. To detect watery area, electrical and electromagnetic methods have been introduced ahead for detection. Ground-penetrating radar (GPR) is a widespread nondestructive geophysical technique. Its signals are sensitive to changes in the subsurface, which has electromagnetic property contrasts. Many researchers have used GPR for the detection of water bodies, fissures, and fractured rock ahead of the tunnel face [8–12]. The transient electromagnetic method (TEM) is mainly used in surveying and detecting mineral resources [13, 14]. This method was first introduced in China by Li. After years of development, it has been widely used in tunnel prediction and water-bearing structure detection [15]. Advanced drilling is also a necessary method when high-risk geological

(a) (b)

Figure 1: The condition of the palm surface at DK114+070: (a) karst cave and (b) fillings from the karst cave.

Table 1: Methods for predicting watery karst areas.

Name	Detection distance	Applicable conditions	Advantages	Disadvantages
Tunnel seismic prediction	120 m	Detect karsts, faults, fracture zones, and other structures	Capable of long-distance detection	Not sensitive enough to watery areas
Transient electromagnetic method	40 m	Detect karsts, faults, fracture zones, fissures, and groundwater	Capable of predicting fractured zones, sensitive to conductive water	Easily disturbed by metal structures, cables
Geological radar	30 m	Detect karsts, faults, fracture zones, fissures, and groundwater	Capable of predicting fractured zones, sensitive to conductive water	Easily disturbed by metal structures, cables
Advanced drilling	30 m	Detect karsts, faults, fracture zones, fissures, and groundwater	Ability to drill and analyze directly into the surrounding rock ahead	Time consuming and influenced by the analyst's experience
Advanced drilling combined with industrial endoscopy	0~30 m	Detect karsts, faults, fracture zones, fissures, and groundwater	Time-saving and precise judgment of the surrounding rock ahead	/

structures are detected. When several advanced drilling boreholes have been installed in a tunnel face, the connection can extend the detection range from point detection to volume detection [11, 16, 17]. In watery karst areas, the accuracy of any single prediction method is not very reliable. Therefore, an integrated forecasting system combining multiple detection means should be established.

After detecting watery karst areas, countermeasures should be taken. The constructions of the Seikan tunnel, Xiang'an tunnel, and Denghuozhai tunnel indicated that curtain grouting technology could be a reliable prereinforcement countermeasure for water and mud inrush prevention [18–20]. The grouting design must consider major factors, such as grouting thickness, grouting material, and grouting technique. The grout thickness should meet the requirements of the tunnel water surge. Numerical modeling has the advantage of analyzing the water inflow in various geological conditions, which has been widely used by many researchers [21, 22]. Zhang et al. analyzed the grouting parameters of the Yong-Lian tunnel using COMSOL and concluded that grouting thicknesses exceeding 8 m were no longer effective for the increase of the water-stopping effect [23]. Li et al. used 3DEC to analyze the sprouting and expansion pattern of cracks in Jingzhai tunnel with different curtain grouting thicknesses and concluded that grouting thicknesses of 5-7 m could control the development of cracks [24]. Shi et al. used ABAQUS to analyze the grouting thickness of the Doumo tunnel and concluded that a grout thickness of 4 m would meet the needs of the project [25]. Liu et al. proposed a coupled seepage-erosion water inrush model and concluded that a grouting thickness of 6 m is suitable for fully weathered granite [26]. These cases show that the evaluation index of grouting effectiveness should be referenced by the amount of water surge. However, different tunnels have different drainage designs, so the specific grouting thickness should depend on the project's own needs. The grouting materials should possess certain groutability so that the slurry can penetrate the ground [27]. The grouting technique needs to solve technical problems such as poor hole formation and difficult slurry diffusion. In recent years, field tests have become the main way to optimize details of curtain grouting. Liu et al. proposed guidelines for injection

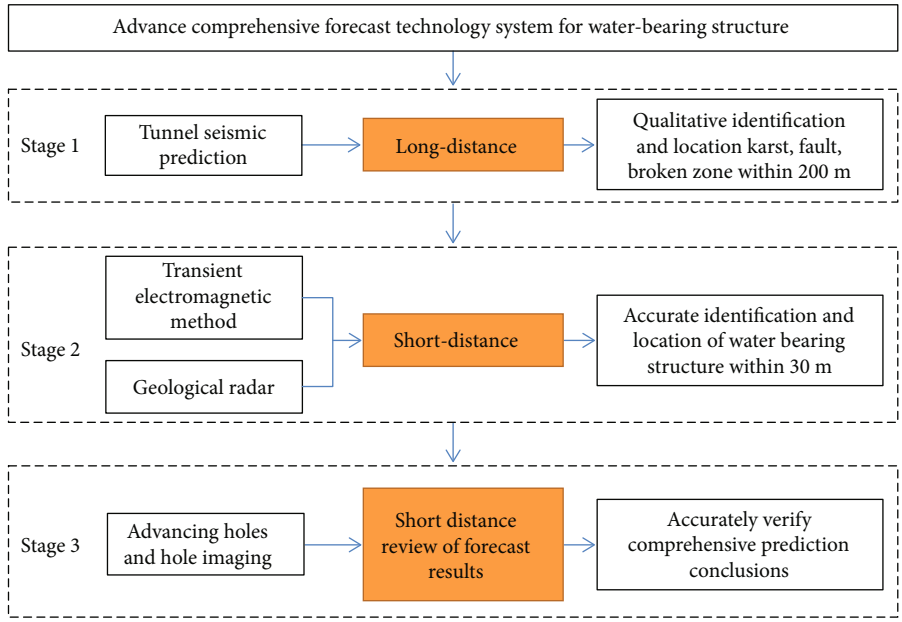

Figure 2: Integrated geological forecasting system.

material selection and grouting volume per meter for various flowing water environments encountered during grouting [28]. Yuan et al. integrated the use of steel pipes for supplemental grouting in collapsed boreholes and dynamic optimization of grouting methods to solve the severe water ingress and collapse problems encountered during drilling and grouting work [29]. Niu et al. performed supplemental grouting in areas of weak grouting based on the complementary detection results [30]. However, these cases are mainly focused on fully weathered granites. Limestone is susceptible to water erosion and the formation of karst caves. Currently, there are few cases of field grouting for limestone.

This paper introduces the comprehensive management method for the watery karst area of Sangujian tunnel. Before excavation, a comprehensive geological forecasting system was established in combination with industrial endoscopy to forecast the extent of the watery karst area. Then a numerical model with six groups of different grouting thicknesses was established by MIDAS-GTS for calculation and analysis. During grouting, the combination of the three grouting techniques can effectively solve the problems of high water surges and difficult hole formation. The principle of "combination of exploration and injection" was followed to obtain real-time geological information and optimize the subsequent grouting plan. After the grouting, the grouting evaluation results and the field construction conditions showed that the grouting effect was good.

2. Engineering Background and Integrated Geological Forecasting System

2.1. Engineering Background. Sangujian tunnel is located in a tectonic low mountain area, which is a Huangshan-derived mountain. The terrain is undulating. The elevation of the mountain ranges from 252 m to 420 m, with a maximum height difference of about 160 m. The mountain is a monoclinic structure. The slope is steeper on the south and north side. The total length is 1235 m.

Tunnel rock layers mainly include the following: the surface layer is mainly the residual slope deposit of the Holocene of the Fourth Series; the bedrock is mainly carbonaceous mudstone of the Lower Cambrian Hetang Formation, the siliceous rock of the Upper Earthquake Piyuan Village Formation, shale of the Middle Earthquake Lantian Formation, and siltstone of the Middle Earthquake Huoning Formation.

The site has a subtropical monsoon climate. The four seasons are distinct. The average annual temperature is 16.1∘C. The frost-free period is 214 days. Under the action of monsoon circulation, there are many rainy days in summer. The annual average precipitation is 161 days. The average precipitation is 1780.7 mm. The maximum annual precipitation is 2511.6 mm. The minimum annual precipitation is 1215.5 mm. According to the analysis, Yixian County, Huangshan City area produces nearly 18×10^5 m^3 of water per square kilometer, which is as much as 2.0 times the provincial average and 3.8 times the national average. Although water resources are abundant, the spatial and temporal distribution of precipitation is extremely uneven. In June of the rainy season, the average precipitation reaches 335 mm, accounting for 19% of the annual precipitation. In September, the average precipitation in the autumn drought is only 96.0 mm, accounting for only 5.5% of the annual precipitation. The precipitation varies greatly throughout the year.

When the tunnel was excavated to DK114+070, a semi-filled cave developed in the vault of the palm face. After the filling collapsed, a vertical cylindrical cave with a diameter of 2~3 m and a height of 4~5 m was formed at the top of

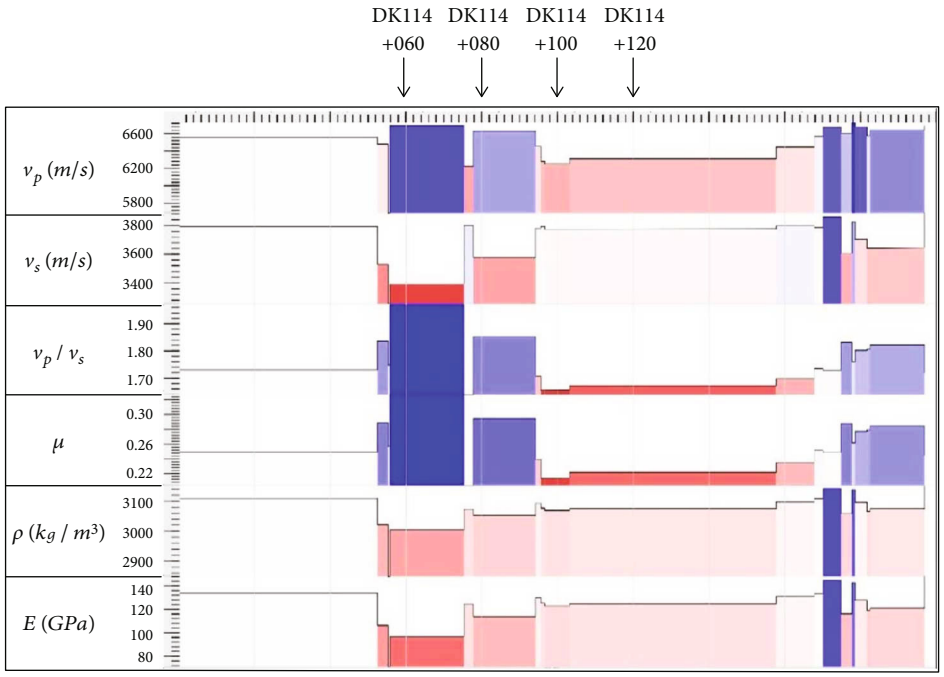

(a)

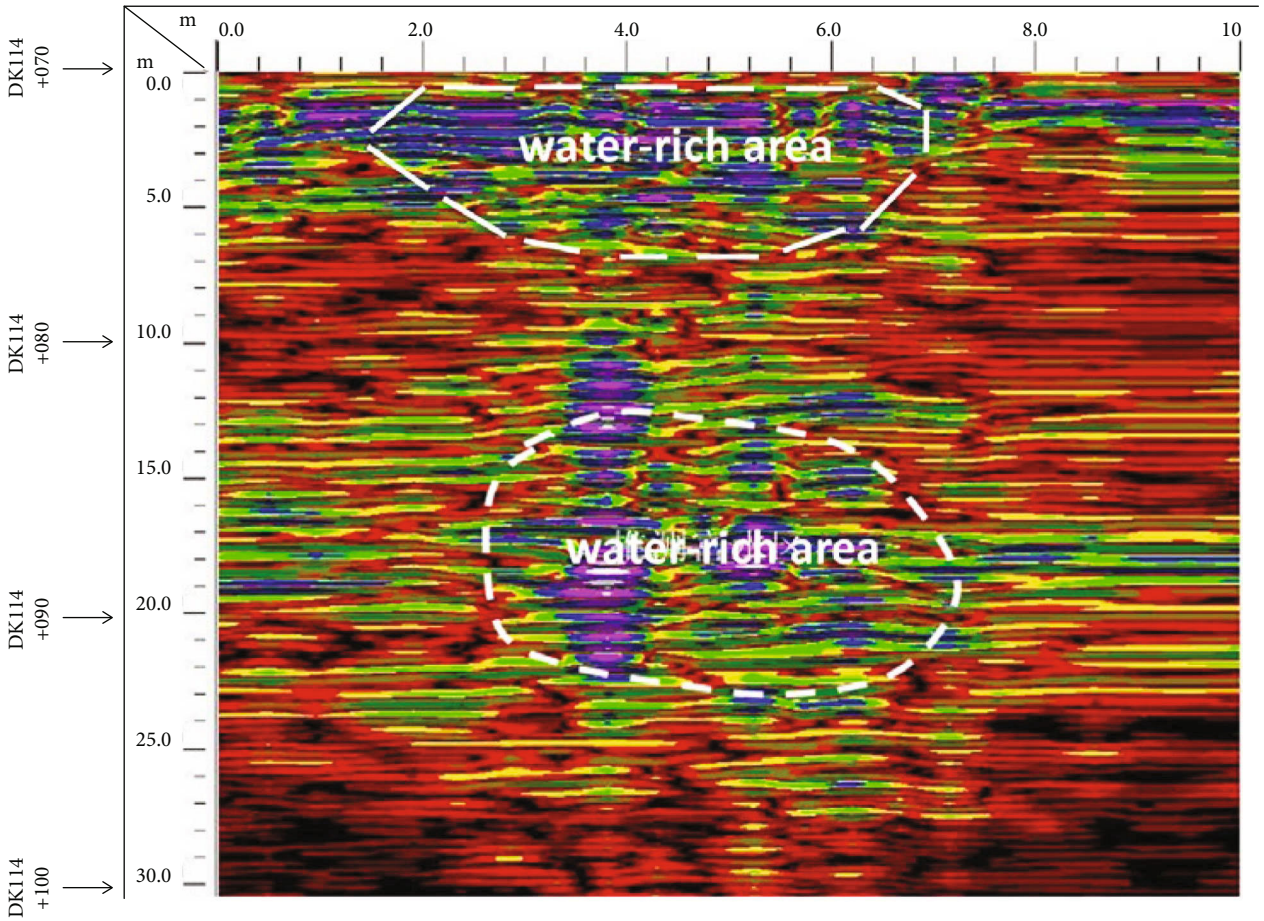

(b)

Figure 3: Continued.

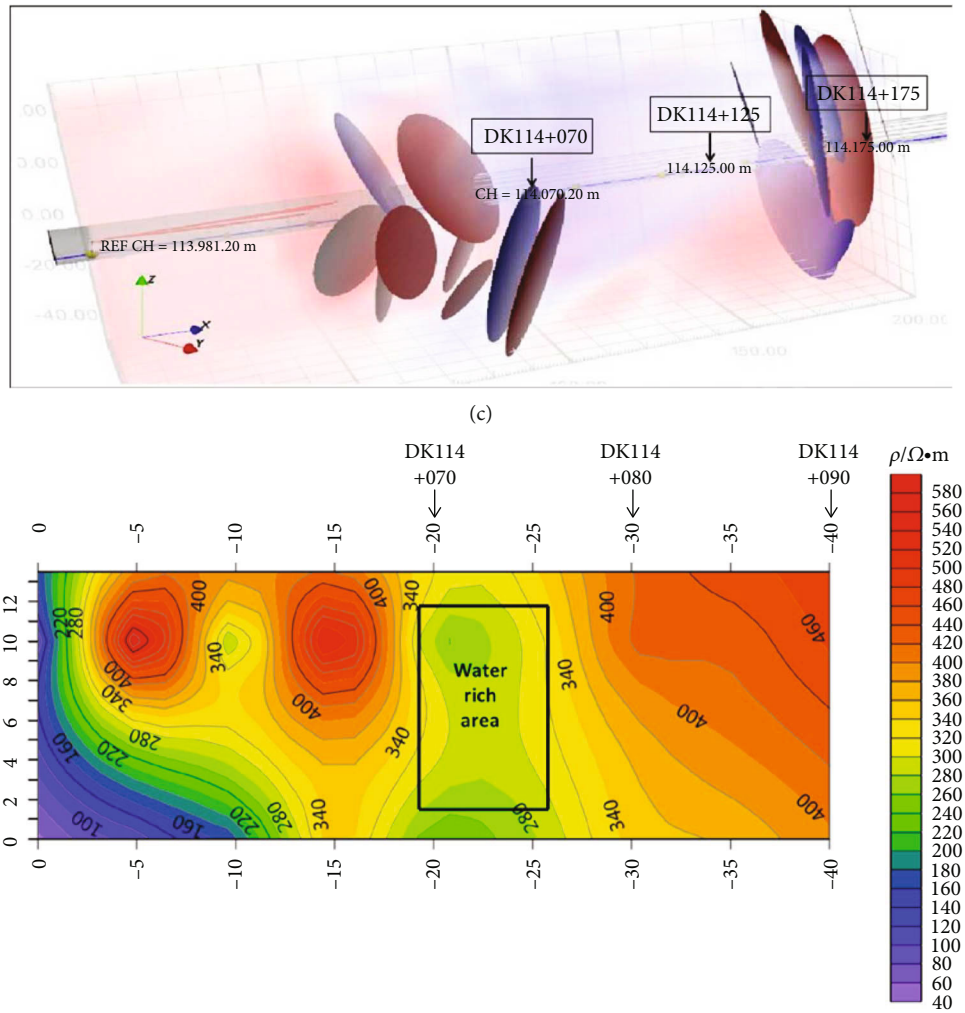

Figure 3: Integrated geological forecast results: (a) physical and mechanical parameters; (b) V_P and V_S decomposition of 3D seismic model; (c) results of geological radar; (d) results of transient electromagnetic method.

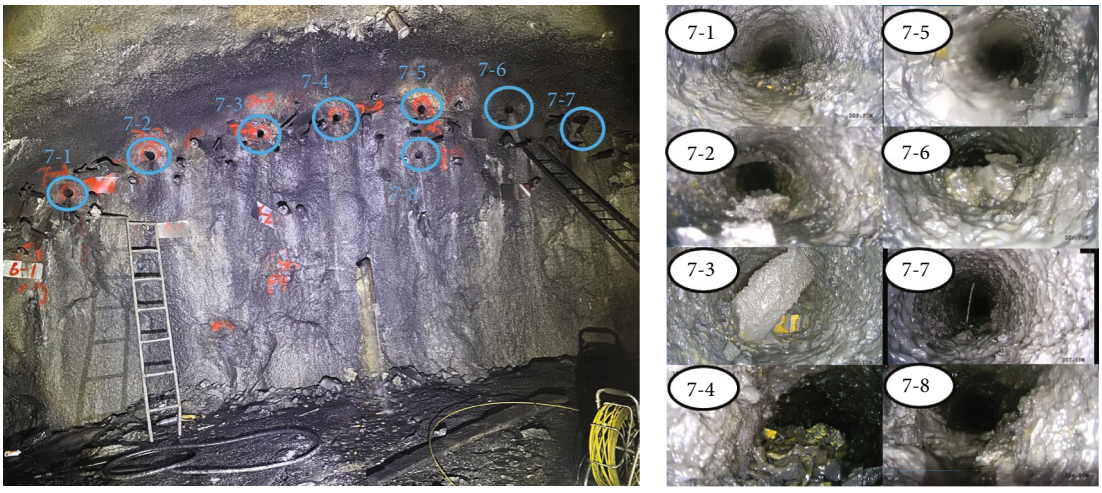

Figure 4: The layout and imaging results of last drills: (a) layout and (b) imaging results.

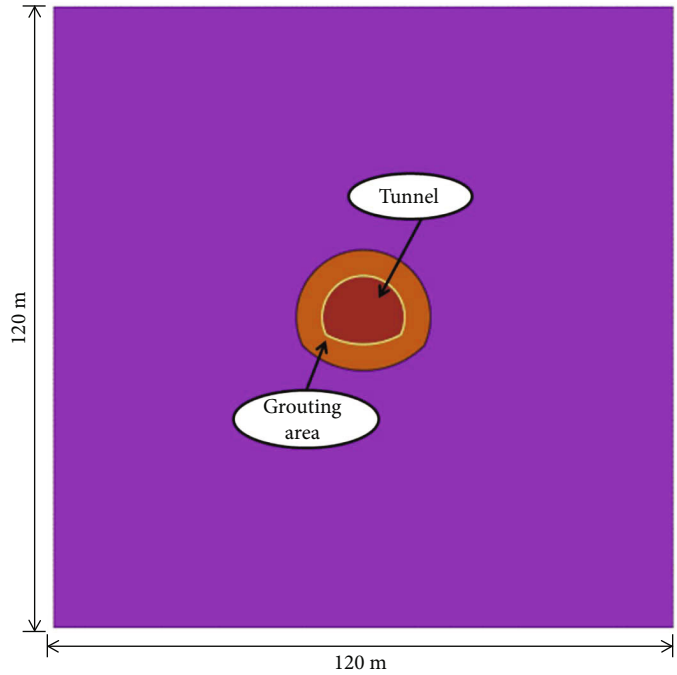

Figure 5: The 2D calculation model.

the tunnel arch (Figure 1). The excavation revealed that the lithology is weakly weathered striped tuff. The lithology is nearly horizontal, thin to medium laminated. The interlayer is filled with white calcite powder, which is poorly bound and soft. The rock is fragmented and the joints and fissures are developed due to tectonic compression.

The initial program adopted Forward Grouting Technology to reinforce the surrounding rock in front. However, after completing the grouting of 149 holes, the phenomenon of collapse in holes still existed in the holes. The rock in front is a soft and hard uneven accumulation after dissolution, mainly composed of soft plastic sandy clay, soft rock mass, and dissolved residual calcareous nodules. The karst fissures can be seen between the cement slurry filling body which has become smooth. The karst fissures are linear in shape. Excavation may induce deformation of the surrounding rock and sudden water and mud disasters. Therefore, a more detailed geological forecast was carried out.

2.2. Integrated Geological Forecasting System. To accurately identify the information of the watery karst area in front of the palm face, a reasonable prediction method must be selected according to the actual geological conditions and problems. Table 1 lists the applicable conditions and advantages and disadvantages of the commonly used advanced geological prediction techniques.

Through comparison and analysis, the prediction focus of each method is found to be different. TSP can be used to identify and locate undesirable geological formations over long distances but is not sensitive enough to identify water bodies. The transient electromagnetic method or ground-penetrating radar method is more sensitive to the response of conductive water bodies but is susceptible to the interference of the whole tunnel space and complex electromagnetic environment. Therefore, these two methods need to be combined and mutually verified to improve the reliability and accuracy of water body identification. The drilling method can directly drill and core the surrounding rock in front of the analysis, so as to verify the geophysical exploration results. However, this method is still stuck in the "drilling first and analyzing later" stage. The conclusion of the analysis is highly dependent on the experience of the analyst. There is also a time lag in the final report. In order to get more accurate verification results, industrial endoscopy technology is applied to the drilling method. Through real-time video observation of the borehole wall, lithology, and water emergence points in the borehole, the geological situation in front of the palm face is timely understood. It can effectively improve the accuracy of geological forecasting and shorten the time to produce results.

Through the above analysis, a comprehensive prediction system for water-bearing faults was established according to the principle of "from far to near and multiple prediction methods verifying each other", as shown in Figure 2. The system makes full use of the advantages of various methods and combines them in a scientific and reasonable way. It realizes the complementary detection range and accuracy and greatly improves the accuracy of prediction results.

2.2.1. Tunnel Seismic Prediction. The TSP303PLUS tunnel geological forecasting system developed and produced in Switzerland was used. The detection range is DK114 +070~DK114+190. The detection results are shown in Figures 3(a) and 3(b). The longitudinal velocity (V_S) and transverse velocity (V_P) of DK114+070~DK114+078 remain almost the same. The value of V_P/V_S has a large increase,

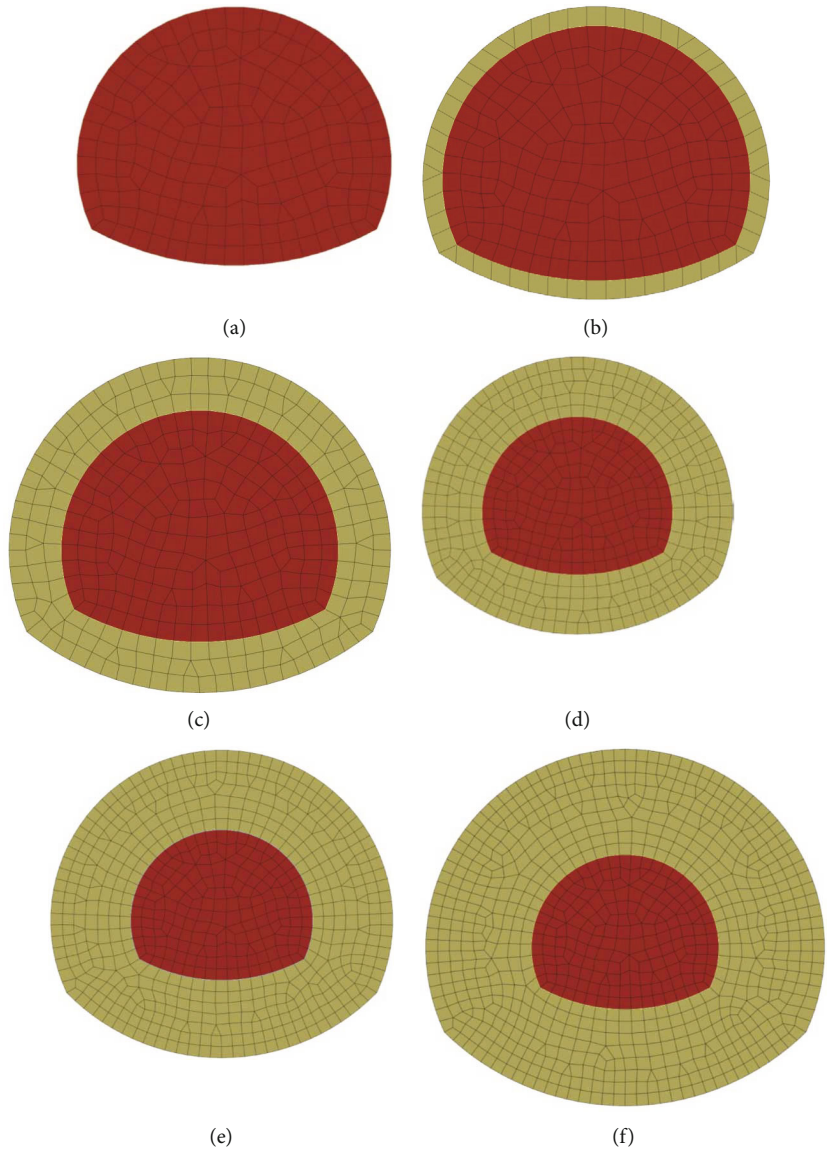

Figure 6: The model diagram of the thickness of the grout: (a) no grouting, (b) grout 1 m, (c) grout 3 m, (d) grout 5 m, (e) grout 7 m, and (f) grout 9 m.

Table 2: Material parameters.

	Density/ (kg/m^3)	E/ GPa	μ	c/ kPa	$\varnothing$/ (°)	Permeability coefficient	Constitutive model	Element type
Surrounding rock	2000	1	0.4	100	20	2×10^{-6}	Mohr—Coulomb	Plane strain
Grouting area	2200	1.3	0.4	150	30	4×10^{-8}	Mohr—Coulomb	Plane strain
Initial support	2450	25	0.2	/	/	/	Flexibility	Beam

and its value is >1.73. There is a sudden change in Poisson's ratio, and there is an obvious reflection interface between DK114+076~DK114+078. There is a sudden change in Poisson's ratio, and there is an obvious reflection interface between DK114+076 and DK114+078. It is assumed that the surrounding rocks in this section basically continue the current geology of the palm face, and the lithological contact zone between carbonaceous tuff and siliceous rocks may be in the range of DK114+076 to DK114+078. The value of V_P/V_S ratio is significantly higher, and its value is >1.73. Poisson's ratio is decreasing, and rock density is increasing. It is presumed that this area is under the influence of a

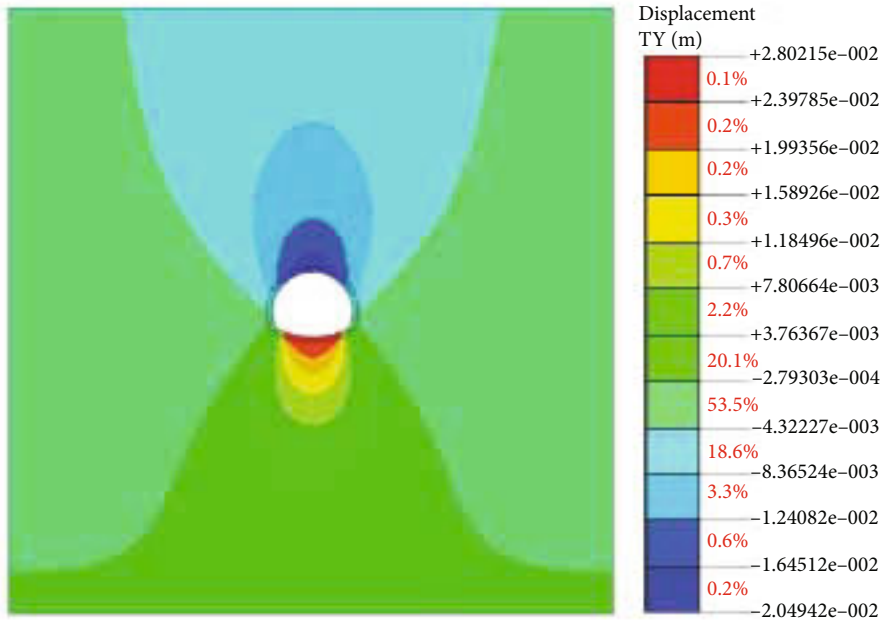

(a)

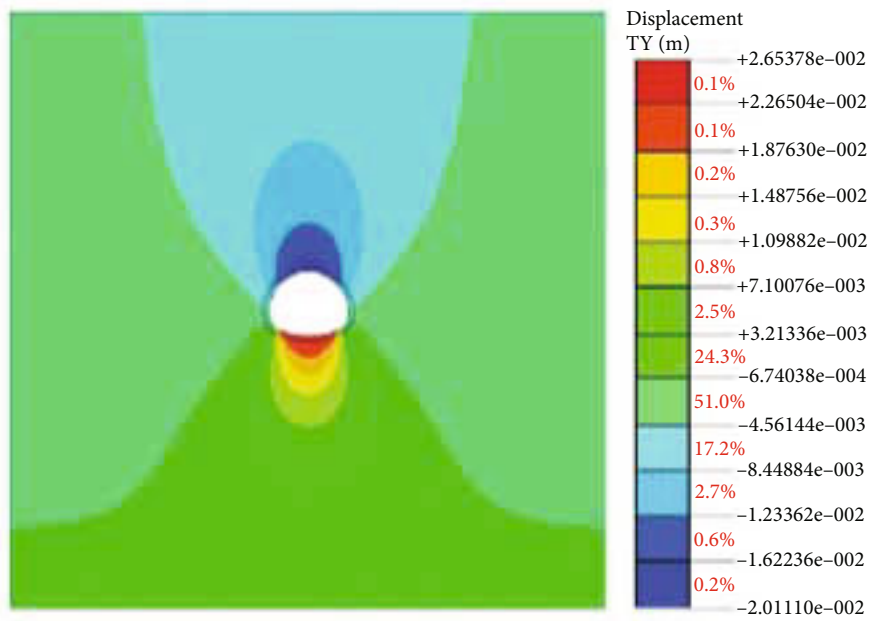

(b)

Figure 7: Continued.

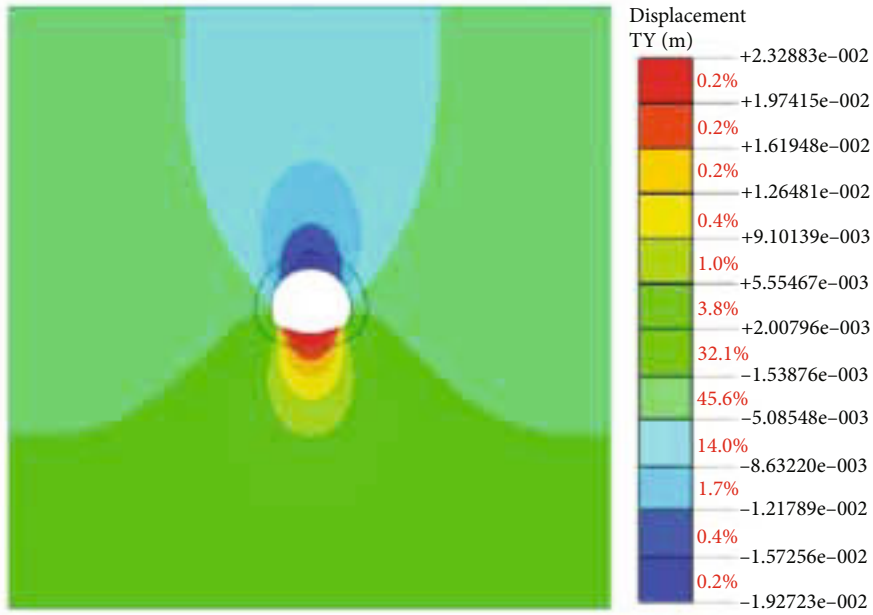

(c)

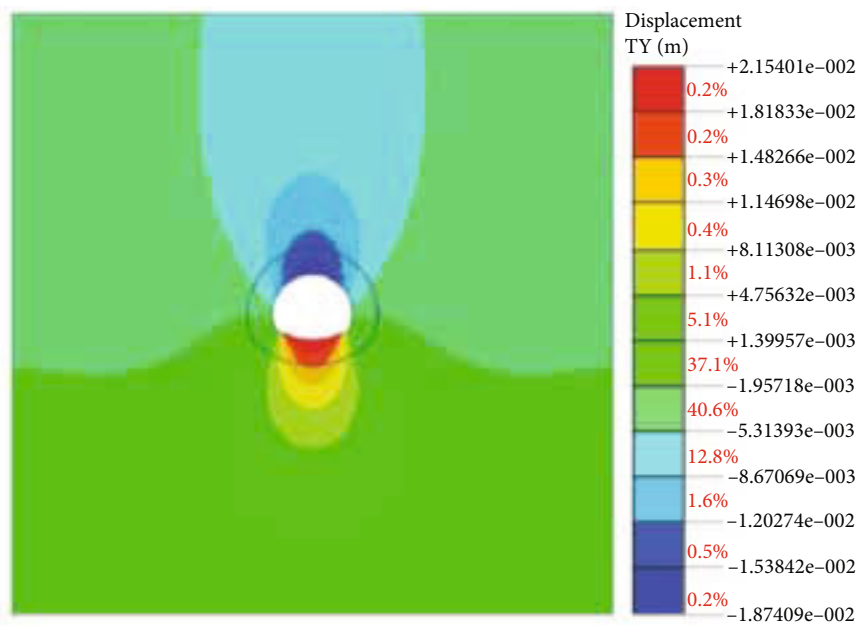

(d)

Figure 7: Continued.

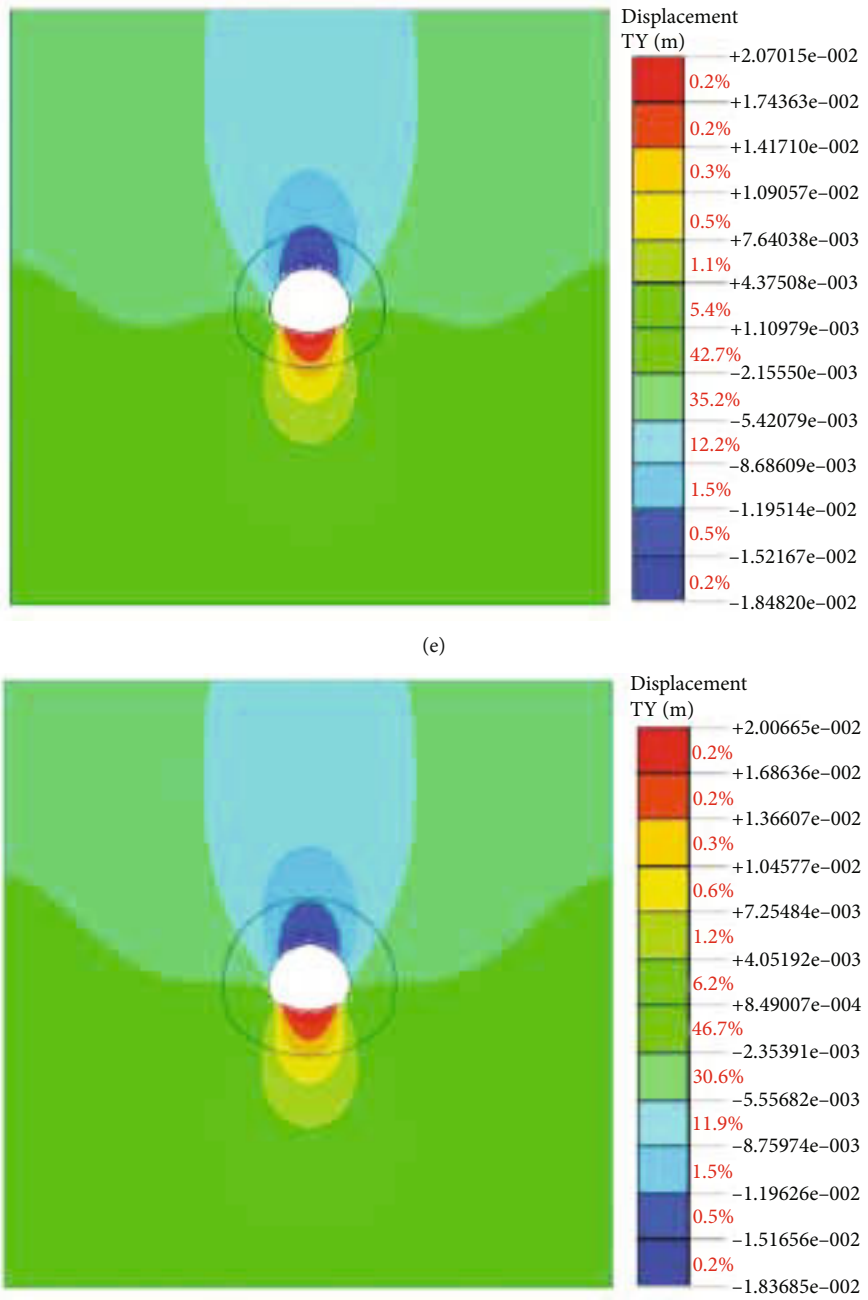

Figure 7: Vertical displacement cloud of the tunnel: (a) no grouting, (b) grout 1 m, (c) grout 3 m, (d) grout 5 m, (e) grout 7 m, and (f) grout 9 m.

lithological contact zone. The longitudinal velocity of DK114 +095~DK114+168 decreases and the transverse velocity increases. The value of V_P/V_S is 1.73. The Poisson's ratio decreases, and the rock density is basically the same as that of the previous section. There is no obvious reflection interface. The longitudinal velocity of DK114+168~DK114+190 section has increased. The transverse velocity has decreased and fluctuated. The value of V_P/V_S has increased significantly. The value is >1.73. The Poisson's ratio has increased. It is assumed that the surrounding rock in this section basically continues the current geological situation of the palm face. The rock body is broken and the groundwater is developed.

2.2.2. Geological Radar. SIR-4000 geological radar was used. The detection range is DK114+070~DK114+100. The detection results are shown in Figure 3(c). The electromagnetic wave energy group in the DK114+070~DK114+095 section is not uniformly distributed. The waveform is more disordered. Reflected waves are locally misplaced in the same phase axis. It is presumed that the surrounding rock of this section basically continues the current geological situation

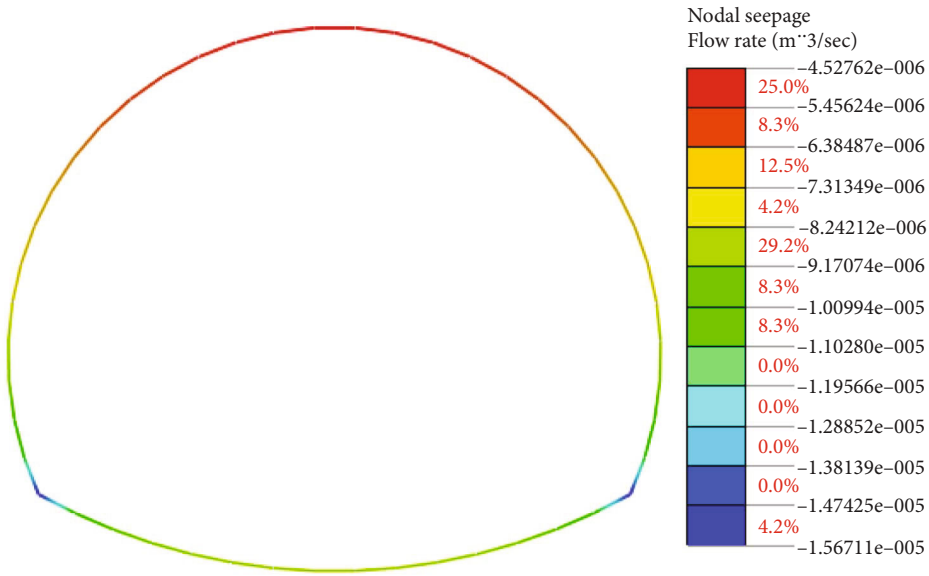

(a)

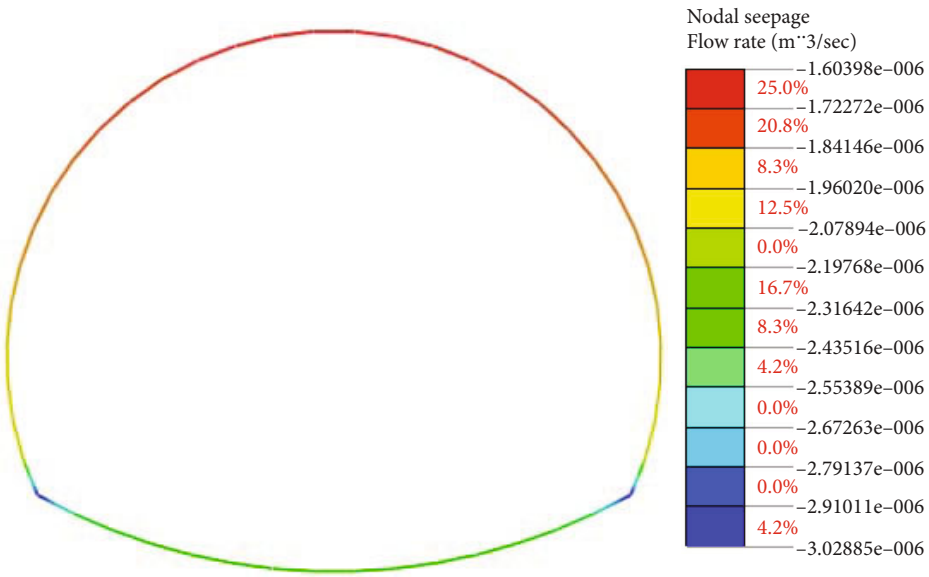

(b)

Figure 8: Continued.

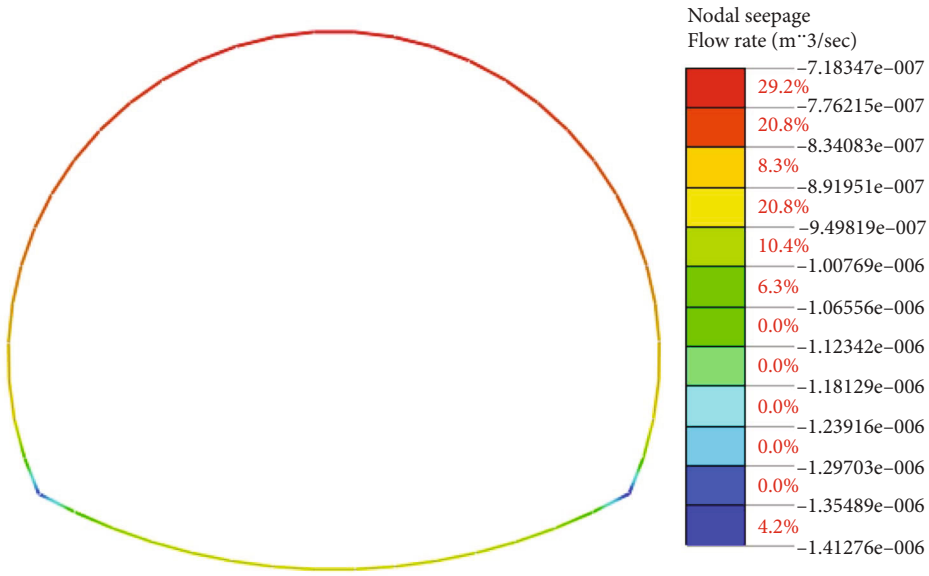

(c)

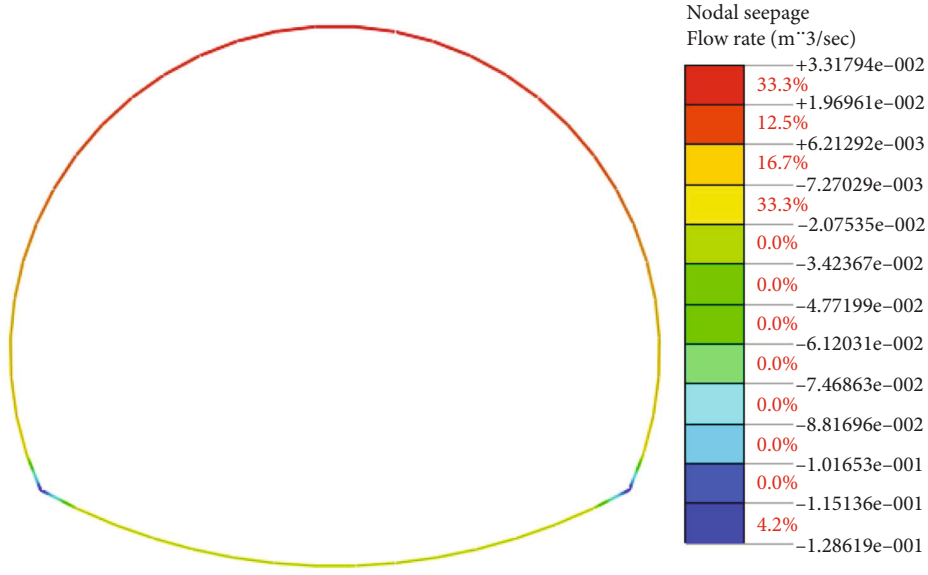

(d)

Figure 8: Continued.

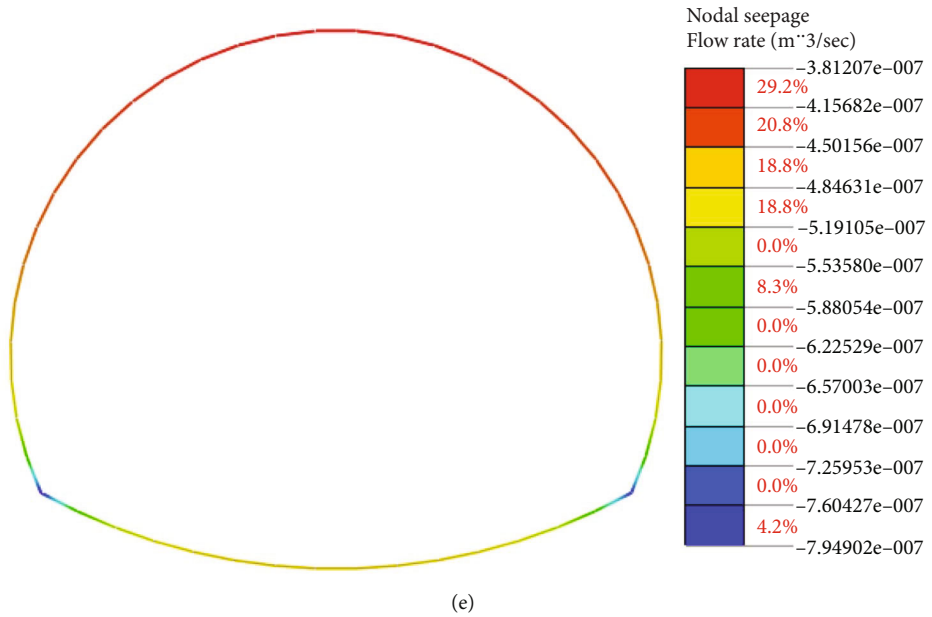

(e)

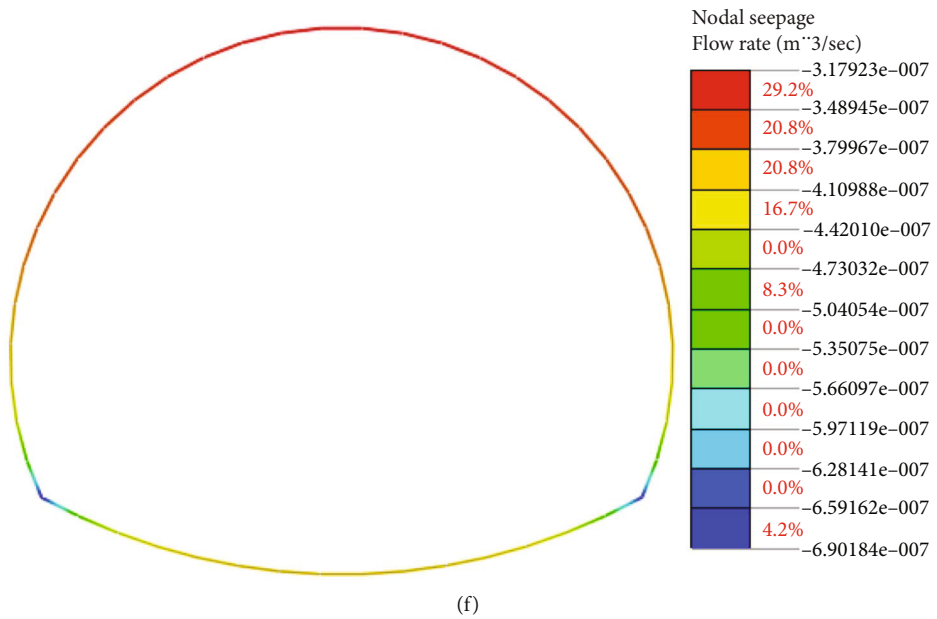

(f)

Figure 8: Cloud map of water surges: (a) no grouting, (b) grout 1 m, (c) grout 3 m, (d) grout 5 m, (e) grout 7 m, and (f) grout 9 m.

Table 3: Water surge per meter of tunnel.

Grouting thickness (m)	0	1	3	5	7	9
Water surge (L/(m•min))	22.14	5.74	2.51	1.71	1.35	1.14

of the palm face. Near the white area, the electromagnetic wave frequency changes drastically from high frequency to low frequency. The pulse period increases significantly. The electromagnetic wave energy decays rapidly. Uneven distribution of energy clusters. The automatic gain gradient is large. And the reflected wave has good continuity in the same phase axis. The waveform is relatively single. It is presumed that the range is the watery area of the rock body. Combined with the TSP detection conclusions, it is presumed that there is a lithological contact zone in this area. The electromagnetic wave energy distribution is more uniform from DK114+95 to DK114+100. The waveform is also more uniform. The reflected waves are clear and continuous in the same phase axis. It is presumed that this section belongs to the influence range of the lithological contact zone.

2.2.3. Transient Electromagnetic Method. An equivalent inverse magnetic flux transient electrometer was used. The instrument was deployed when the tunnel was excavated to DK114+050. The detection range is DK114+050~DK114

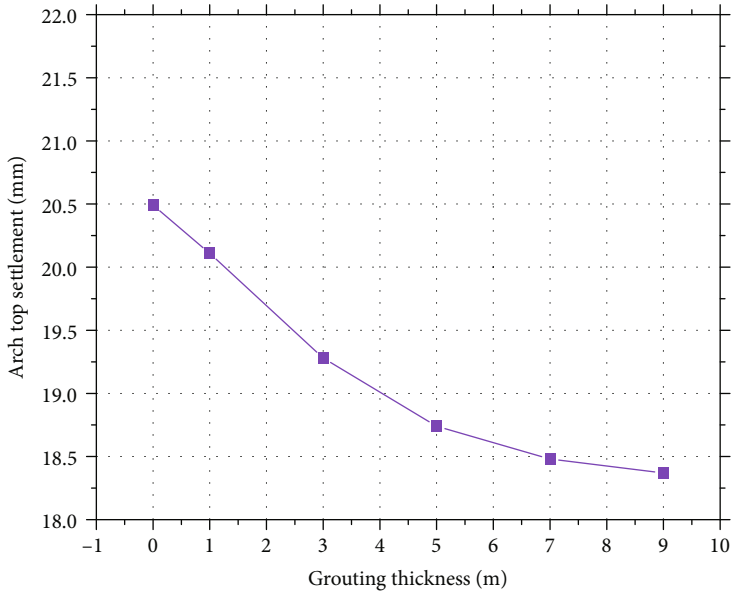

(a)

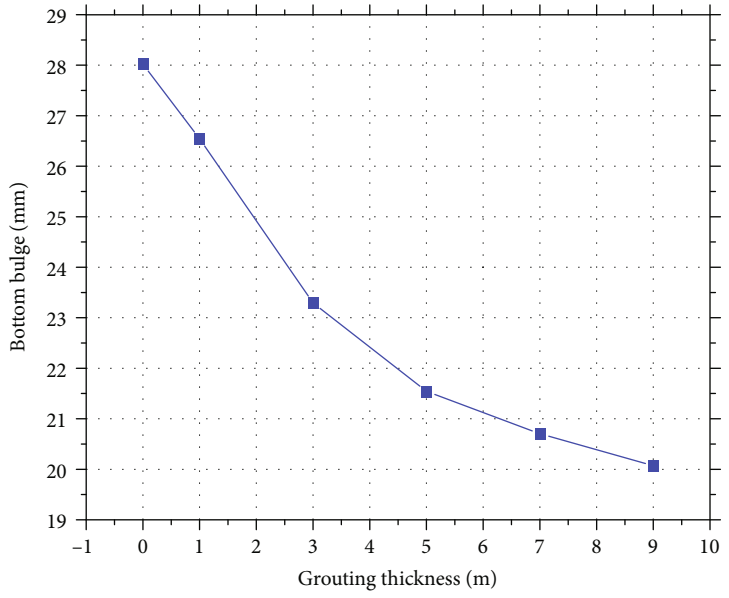

(b)

Figure 9: Continued.

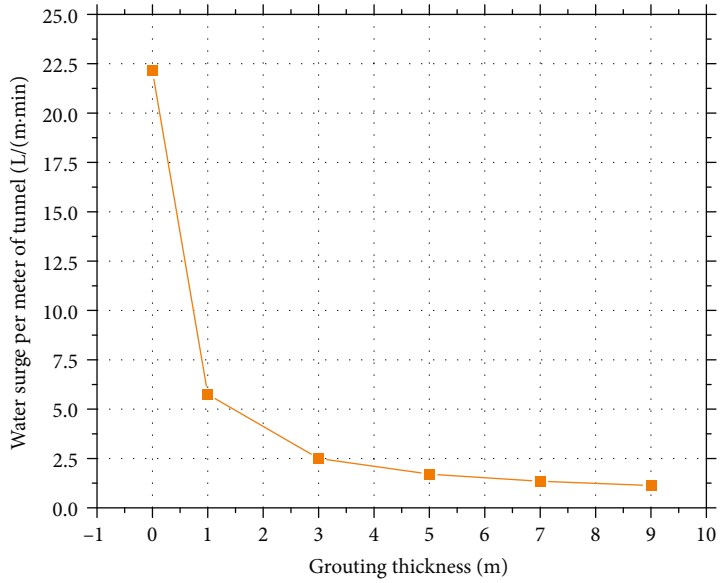

(c)

Figure 9: The control indicators of the tunnel: (a) arch top settlement, (b) bottom bulge, and (c) water surge per meter of the tunnel.

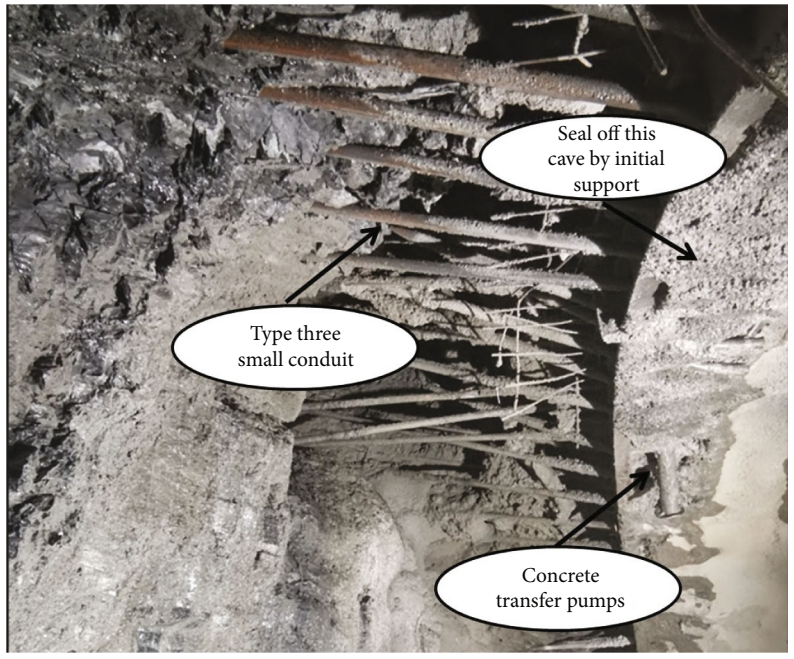

Figure 10: Treatment measures for the cave.

+090. The resistivity inversion cross-section of the lateral line is shown in Figure 3(d). According to the results of this completed detection, there is an obvious low resistance anomaly area in the range of DK114+070~DK114+075. It is presumed that the rock in this area is broken and watery, and there may be some scale of cave occurrence.

2.2.4. Advanced Drilling Combined with Industrial Endoscopy. Of the 149 holes in the forward grouting, in-hole imaging was completed for 53 of them. A total of 8 holes were imaged in the last in-hole imaging. The layout and imaging results are shown in Figure 4.

Hole 1 was drilled for 11 m. A slight collapse occurred at 4 m. A serious collapse occurred at 8.5 m. Hole 2 was drilled for 12 m. A slight collapse occurred at 2.5 m. A serious collapse occurred at 5.5 m. Hole 3 was drilled for 12 m. Slight collapses occurred at 2 m, 3.8 m, and 6.3 m. A serious collapse occurred at 8.5 m. Hole 4 was drilled for 15 m. Slight collapses occurred at 3 m, 7 m, and 9 m. Hole 5 was drilled for 15 m. Slight collapses occurred at 1 m, 2 m, and 3.5 m.

Table 4: Grouting parameters.

Parameter name		
Grouting range	Length	Grout injection 25 m (including stop wall) Excavation length 20 m (including slurry stop wall), set aside 5 m as a safety rock pan
	Thickness	
Diffusion radius of the slurry		1.5 m
Final pressure of the grouting		3.0~5.0 MPa
Diameter of grouting holes		Φ90mm, Φ130 mm
Grouting speed		10~90 L/min
Spacing of the final hole		≤2.3 m
Grouting technology		Combination of forward segmental grouting, backward segmental grouting, and cluster cuff tube grouting
Number of grouting holes		130
Tube of orifice		L = 1.5 m. Φ108 mm. 6 mm thickness

A serious collapse occurred at 10 m. Hole 6 was drilled for 15 m. Slight collapses occurred at 2.6 m and 5 m. A serious collapse occurred at 6.8 m. Hole 7 was drilled for 15 m. Slight collapses occurred at 3 m, 5.4 m, and 7 m. A serious collapse occurred at 11.3 m. Hole 8 was drilled for 18 m. Slight collapses occurred at 2.5 m, 4.3 m, and 5 m. A serious collapse occurred at 13.6 m.

According to the imaging results in the hole, the preliminary judgment of the palm face in front of the 0~13.6 m range of rock body is extremely broken. Combining the results of tunnel seismic prediction, transient electromagnetic method, and georadar, it is presumed that the surrounding rocks of DK114+070~DK114+095 in front of the palm face are basically consistent with the current geology of the palm face.

3. The Numerical Simulation of the Curtain Grouting

3.1. Physical Model. To obtain a reasonable grouting thickness, a two-dimensional computational model for stress-percolation coupling was built in MIDAS GTS. The width and height of the model are 120 m. The tunnel is located in the middle of the model, satisfying the St. Venant principle. The model schematic is shown in Figure 5. Six different analysis conditions are set up: no grouting, grout 1 m, grout 3 m, grout 5 m, grout 7 m, and grout 9 m. The schematic diagram of the model with different grouting thicknesses is shown in Figure 6.

The boundary conditions are as follows. Fixed constraints are added to the bottom of the model. Horizontal constraints are added to the sides of the model. The actual burial depth of the tunnel is about 130 m. The top of the tunnel is about 60 m from the upper boundary of the model. According to the self-weight stress formula, an equivalent vertical load is applied on top of the model: $q = 20 \times (130 - 60) = 1400$ kPa. The water seeping through the reinforcement ring into the lining is then discharged through the lining drainage system. Therefore, the water pressure on the lining is set to zero. According to the hydrogeological conditions of the site, the water level height was set at 50 m above the tunnel. The surrounding rock area, grouting area, and tunnel area are all set up as plane strain models. The initial support is set up as a beam unit model and follows the elasticity criterion. The secondary lining is often used as a safety reserve in tunnel design, so it is not considered in this model.

3.2. Model Parameters. In the finite element analysis software MIDAS GTS, the physical and mechanical parameters of the surrounding rock in the enhanced grouting zone are usually used to equate the effect of grouting. Combined with the site engineering geological data, the density, elastic modulus, cohesion, and internal friction angle of the grouted area are increased to 1.1 times, 1.3 times, 1.5 times, and 1.5 times of the original values, respectively [31, 32]. Reducing the infiltration coefficient in the grouted area to 2% of the original is an economical and reasonable choice [33]. The physical parameters of the materials are shown in Table 2.

3.3. Simulation Results

3.3.1. The Effect of Grout Circle Thickness on Tunnel Deformation. The arch top settlement displacement and arch bottom bulge displacement are important to control indicators during tunnel excavation. After the construction is completed, the vertical displacement cloud of the tunnel is shown in Figure 7.

For the arch top settlement, the value without grouting is 20.49 mm. During the process of increasing the grouting thickness from 1 m to 9 m, the arch top settlements are 20.11 mm, 19.28 mm, 18.74 mm, 18.48 mm, and 18.37 mm, which are reduced by 1.85%, 5.91%, 8.54%, 9.81%, and 10.35%, respectively. For the arch bottom bulge, the value without grouting is 28.02 mm. During the increase of grouting thickness from 1 m to 9 m, the arch top settlements are 26.54 mm, 23.29 mm, 21.54 mm, 20.70 mm, and 20.07 mm, which are reduced by 5.28%, 16.88%, 23.13%, 26.12%, and 28.37%, respectively.

3.3.2. The Effect of Grouting Circle Thickness on Tunnel Water Gushing. Generally speaking, curtain grouting of tunnels is not only to change the physical parameters of the surrounding rock but also to reduce the deformation of the

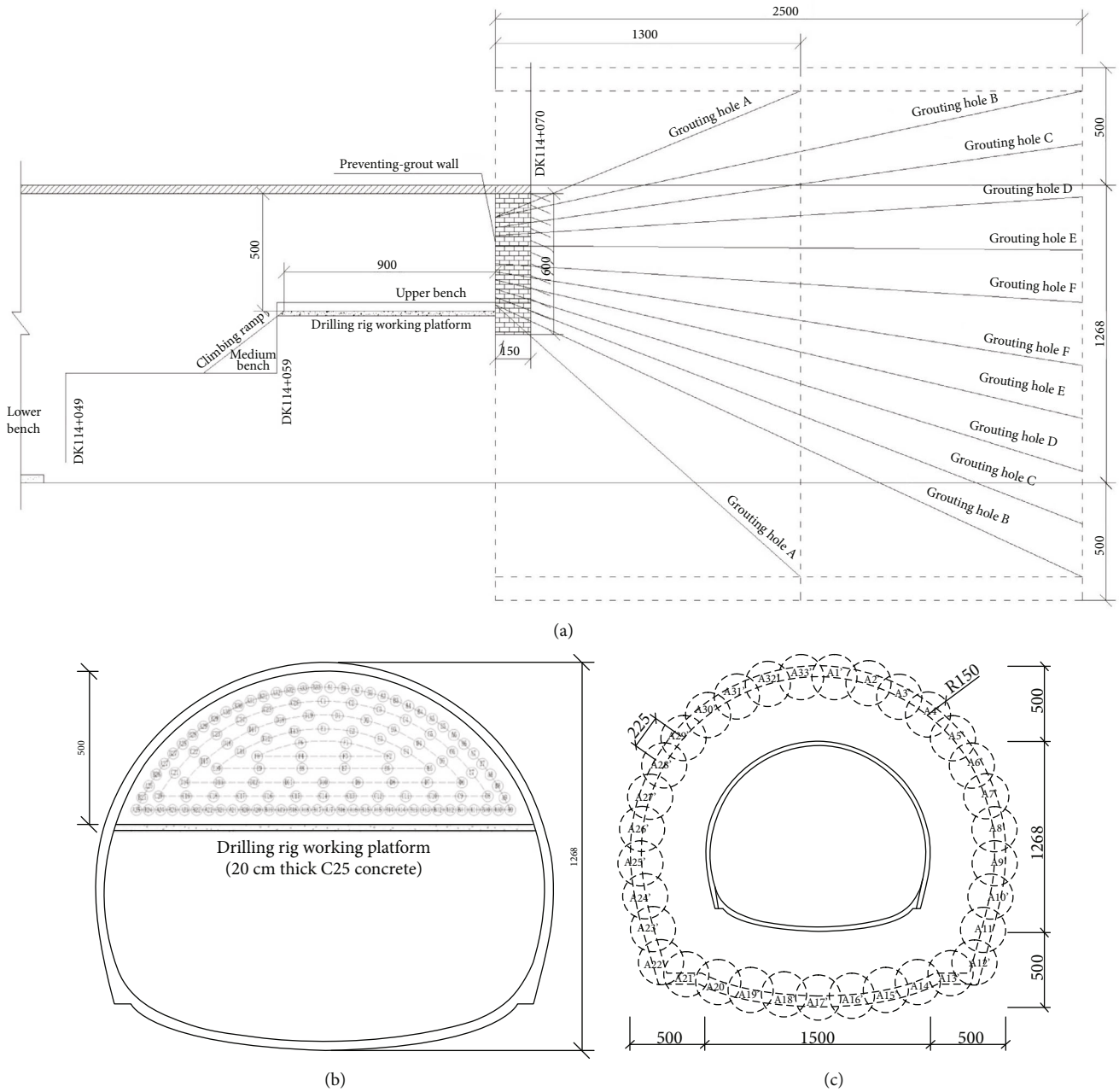

Figure 11: Continued.

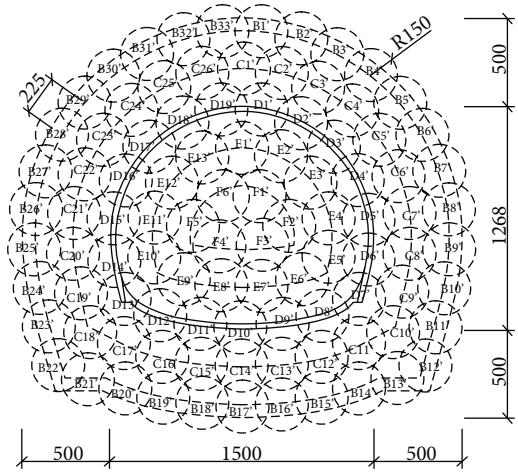

(d)

Figure 11: Layout of grouting boreholes: (a) longitudinal profile, (b) cross-section, (c) supplementary cross-section, and (d) final cross-section.

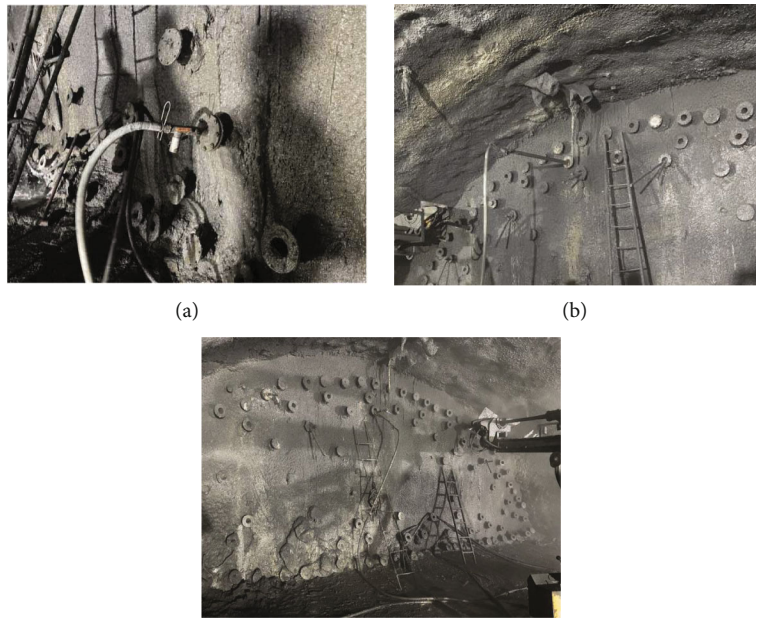

(a) (b)

(c)

Figure 12: Grouting technology: (a) Forward Segmental Grouting, (b) Backward Segmental Grouting, and (c) Cluster Cuff Tube Grouting.

tunnel. Most importantly, it can limit the gushing of water from the surrounding rock into the tunnel. Different grouting thicknesses of the case of the tunnel surge water cloud map are shown in Figure 8. From Figure 8, it can be found that in the absence of grouting and full-section curtain grouting, the maximum amount of water surge in the tunnel is found at the foot of the arch. The tunnel contour line on all nodes of the water surge summation and the tunnel unit length of the water surge can be attained, as shown in Table 3. The water surge without grouting is 22.14 L/(m•min). During the process of increasing the grouting thickness from 1 m to 9 m, the water surge is 5.74 L/(m•min), 2.51 L/(m•min), 1.71 L/(m•min), 1.35 L/(m•min), and 1.14 L/(m•min), which are reduced by 74.06%, 88.68%, 92.29%, 93.91%, and 94.87%, respectively.

3.3.3. Grouting Ring Thickness Selection. The numerical simulation results are plotted as dotted line plots, as shown in Figure 9. It is not difficult to find that with the enhancement of the grouting thickness, the deformation and water surge of the tunnel can be effectively limited, especially the water surge of the tunnel. It can be seen that the grouting has a very obvious effect on reducing the water surge of the tunnel. However, the thickness of the grouting is not as large as possible.

Figure 13: Use sulfoaluminate cement for grouting hole B28.

From Figures 9(a) and 9(b), after the grouting thickness exceeds 5 m, it can be found that the curve starts to become flat. This indicates that the effect of grouting on limiting tunnel deformation is weakening. Mechanistically speaking, after the tunnel is excavated, the main influence is on the rock body within a certain area around the tunnel. After the tunnel is supported, the support structure and the rock surrounding the tunnel form the support system of the tunnel. The better this part of the rock mass around the tunnel, the smaller the force borne by the support structure. When the grouting range exceeds this part, the remaining rock mass has less influence on the force of the support structure. Therefore, improving the parameters of rock masses outside this part has little significance to the force of the support structure.

From Figure 9(c), after the grouting thickness exceeds 3 m, the curve starts to become flat. This indicates that the water-stopping effect of grouting on the tunnel is decreasing rapidly. After the grouting thickness exceeds 5 m, the water-stopping effect of the tunnel almost stops increasing. At this point, it can be considered that the increase in grouting thickness is no longer meaningful to improving the water-stopping effect.

Comparison of the displacement limitation effect and water-stopping effect, the curtain grouting thickness is mainly reflected in reducing the amount of water surge, while the improvement of the displacement of the tunnel support structure is slightly weaker. Therefore, when determining the thickness of grouting, the water seepage should be the main reference basis. When the grouting thickness exceeds 5 m, the water-stopping effect of the tunnel is almost unchanged. Considering the cost, the grouting thickness of 5 m is recommended as a reference value for this project. At this point, the numerical simulation result of the water surge is 1.71 L/(m•min), which meets the design of the tunnel (2 L/(m•min)).

4. Treatment Measures Applied for Watery Karst Area

4.1. Adjusting Construction and Backfilling the Karst Cave. DK114+070~DK114+100 surrounding rock grade is adjusted from grade IV to grade V. The lining type adopts VC type composite lining. Overrun support is adjusted from type I small conduit to type III small conduit. The excavation method is adjusted from a three-step excavation method to a three-step excavation method with a temporary elevation arch. The initial support construction adopts the steel frame of type I22a steel. Steel frame spacing 60 cm. Use Φ22 steel welding. Set up the lock foot anchor pipe (Φ50, $L = 4$ m). Use Φ22 "U" steel welded firmly. Ensure that the grouting is full. Arch feet need to be padded in the through-length channel steel above. Channel steel under the use of concrete pad support. Ensure that the foot of the arch is not the off-air phenomenon.

The cave outside the tunnel contour line was closed with 20 cm thick C25 concrete. Two pipes with a length of about 2-3 m were reserved for pumping concrete during the initial support construction, as shown in Figure 10. C25 concrete was pumped in two stages to backfill the cave. The pumping volume is 72 m^3.

4.2. Main Parameters of Full-Section Curtain Grouting. The main parameters of the full-section curtain grouting technology include the grouting range, slurry type, and grouting technology. The main grouting parameters are shown in Table 4.

4.2.1. Grouting Range. The grouting range was determined based on the conclusion of the advance geological forecast, numerical simulation results, and experience with similar projects. Grouting mileage: DK114+070~DK114+095. The length of longitudinal reinforcement is 25 m (including the

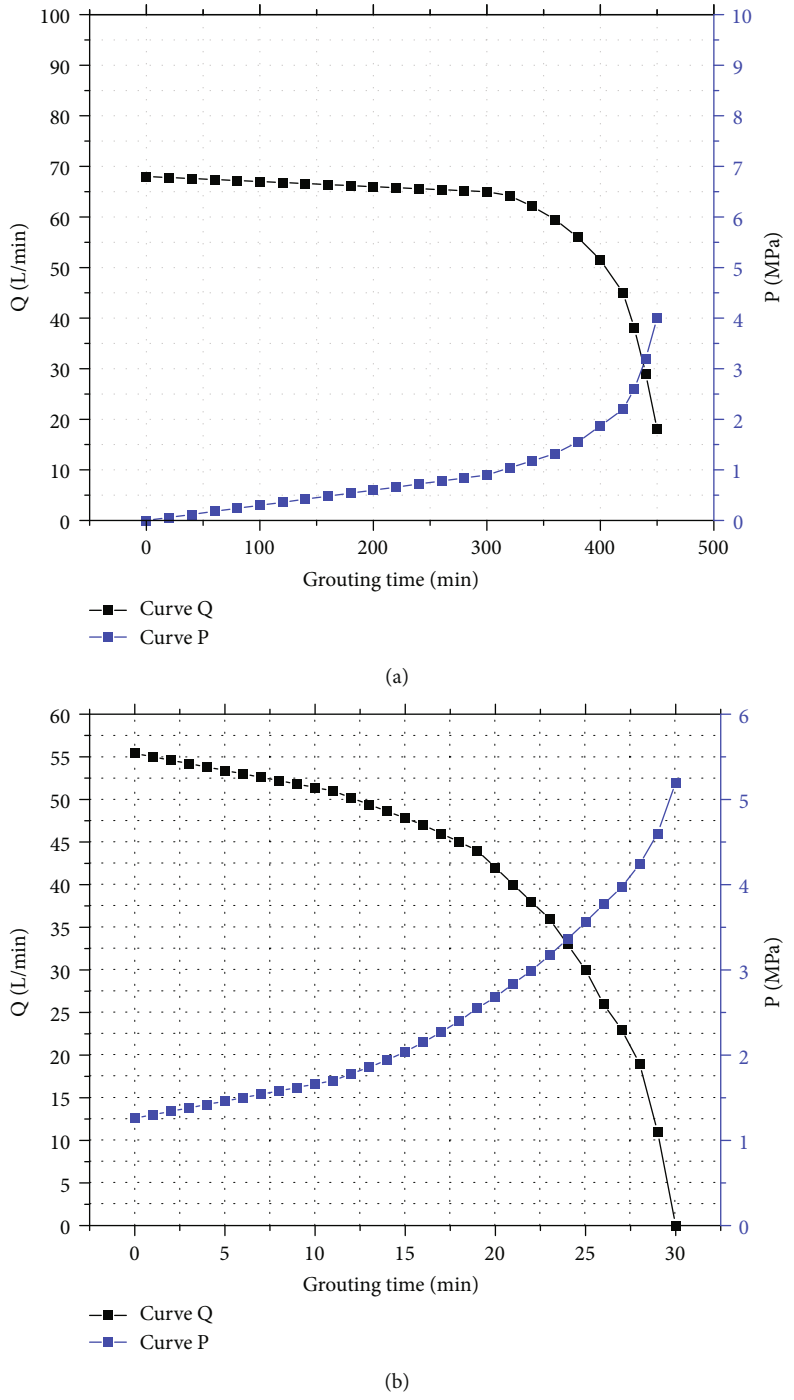

Figure 14: P-Q-T curve: (a) early stage and (b) late stage.

slurry stop wall). The thickness of grouting is 5 m. The excavation length is 20 m. 5 m is reserved as safety thickness. The supplementary section is at 13 m. The final hole section is at 25 m. There are 130 grouting holes in total as shown in Figure 11.

4.2.2. Grouting Materials. The grouting material is mainly sulfoaluminate cement. Cement and cement-sodium silicate are supplemented.

Cement. It is made of ordinary portland cement (P.O. 42.5). The Burning loss rate is less than 5%. The 28-day compressive strength is more than 42.5 MPa. The specific surface area is not less than 300 m^2/kg, and the water-cement ratio is 0.6 : 1~0.8 : 1. The concentration of grouting slurry should be changed step by step from dilute to thick. The water-cement ratio of grouting slurry can adopt 0.8 : 1 and 0.6 : 1. The water-cement ratio at the beginning of grouting can be 0.8 : 1.

(a) (b)

Figure 15: Grouting effect: (a) palm surface after grouting and (b) in-hole imaging of the inspection hole after grouting.

Cement-sodium silicate. The concentration of sodium silicate is greater than or equal to 40° Be. The modulus is controlled between 2.4 and 2.8. The volume ratio of cement slurry and sodium silicate is 1 : 1, and the gelation time is 20 s~30 s.

Sulfoaluminate cement. The water-cement ratio is 0.6 : 1~0.8 : 1.

4.2.3. Grouting Technology. The grouting technology was optimized. A combination of three grouting technologies was used to grout the surrounding rock for reinforcement.

Forward Segmental Grouting. As shown in Figure 12(a), the hole is formed using a drill bit with an orifice tube in the front section to guide positioning. To achieve rapid water plugging and closure and consolidation strength, a fast-hardening sulfoaluminate cement monolithic slurry is pressed and injected. Drilling and grouting are done alternately. Drill holes while grouting. The grouting length was 5-8 m per cycle, and the grouting effect of the implemented holes was verified. This applies to formations with high water surges and good pore formation.

Backward Segmental Grouting. As shown in Figure 12(b), after the initial consolidation of forwarding grouting with hole formation conditions, grouting is carried out in segments from the bottom of the hole for the holes prone to collapse. After drilling to the designed hole depth with the integrated drilling and injection machine, the slurry is injected and the drilling rod is removed section by section (the length of each section is 2~4 m) until the grouting is pushed from the bottom of the hole to the hole entrance. This applies to silty strata and powdery clay that are prone to hole collapse.

Cluster Cuff Tube Grouting. As shown in Figure 12(c), the discount of the grouting consolidation effect in watery areas is considered, and the grouting is controlled and reinforced by cluster cuff tube grouting. It avoids the problem of running slurry caused by the traditional grouting technology in loose strata and the problem of difficulty in compacting in dense strata. Drill holes to design depth using a Φ130 mm drill bit. One to three Φ25 mm rigid cuff pipes can be installed in each hole according to the geological conditions. Intermittently inject cement-sodium silicate or sulfoaluminate cement single-liquid slurry until the design final pressure, according to the water outflow and grouting effect.

4.3. Process of Full-Section Curtain Grouting. Before grouting, a stop wall is first constructed to prevent the grouting slurry from flowing out of the fissure. After the concrete maintenance period of the stop wall, the drilling rig operation platform was constructed. The length of the rig operating platform is 9 m, the thickness is 20 cm, and it is poured with C25 concrete. The top surface of the platform was 5.0 m from the top of the arch, and 0.8 m of concrete was not poured on both sides of the platform and near the slurry stop wall as a drainage ditch. After the construction of the drilling rig working platform was completed, the climbing ramp of the drilling rig was constructed. Then, the drilling rig set up grouting holes and installed orifice pipes according to the design plan. After the preparation work was completed, drilling and grouting started.

During the grouting process, the sequence of curtain grouting is carried out in batches. To avoid drilling string slurry, one hole should be drilled and injected. Combined wind and water flushing or flushing with high flow water through the conduit is used before grouting. Follow the method of flushing from the bottom of the hole to the outside of the hole. Follow the principle of "outside first, then inside, top to down, jumping holes." Follow the construction sequence of "Hole B→Hole C→Hole D→Hole E→Hole F→Hole A."

After the grouting is completed, it will be evaluated using the analytical method and hole inspection method. If the grouting meets the design requirements, the tunnel will continue to be excavated. On the contrary, additional grouting will be performed.

4.4. Construction of Full-Section Curtain Grouting. During the grouting construction, the "combination of exploration and injection" method is used. Specifically, the first series of boreholes should be used as exploration holes to grasp the nature of the surrounding rock and hydrogeological conditions of the area to be treated, to provide a basis for the

construction of subsequent boreholes. According to the stratigraphic conditions, suitable grouting materials and grouting technology should be selected. Continuously modify the key reinforcement area for curtain grouting. For the area with intact surrounding rock and small water output, grouting can be reduced appropriately. For the area with broken surrounding rock and large water output, the grouting volume can be increased appropriately.

During the construction, from the geological situation of the borehole and the water outflow of the borehole, the arch in front of the palm face and on the left side is watery. The integrity of the surrounding rock in the lower half of the section is good, and the water output from the borehole is very small. Among them, the worst part was in hole B28 on the left side of the upper step. In the process of drilling, the water volume in hole B28 suddenly increased when drilling to 25 m. With small pieces of debris flowing out, the water volume was about 18 m^3/h.

Therefore, the grouting plan was optimized. The drilling of hole B28 was stopped immediately and a ball valve was installed to stop the water at the hole. Then the grouting pipe was connected, and the grouting treatment was carried out with sulfoaluminate cement, as shown in Figure 13. The grouting step was strictly controlled in the arch and the left side, and the sulfoaluminate cement single-liquid slurry with a high consolidation rate and short gel time was injected to seal the water path and reinforce the formation. For the lower half of the section, some of the grouting holes were reduced and jump holes were applied. Finally, 81 grouting holes and 6 inspection holes were completed in 22 days. The total grouting volume was 750.25 m^3. 92.05 m^3 of cement-sodium silicate was used. 365.20 m^3 of cement was used. 293 m^3 sulfoaluminate cement was used.

4.5. Grouting Effect of Full-Face Curtain Grouting. After the field grouting was completed, the grouting effect was analyzed and evaluated by analytical method and inspection hole method. The slurry filling rate of the whole excavation surface increased to 89%. The P-Q-T curve (Figure 14) of grouting is by the slurry filling law in fractured stony strata. From the situation of imaging and water output in the hole of six inspection holes (Figure 15), the effect of hole formation is good, and there is no phenomenon of water gushing from the spoil hole. It shows that this cycle of grouting reinforcement and water plugging effect achieves the purpose. The field construction shows that after the end of grouting, the cave rubble filling in the vault has been solidified without the phenomenon of falling blocks after each excavation of 1 circulation. There is no sudden water and mud on the palm surface. At present, the arch top cave has been smoothly transitioned, and the surrounding rock of the palm face has tended to become better now.

5. Conclusions

Countermeasures were taken for the watery karst area of Sangujian tunnel, and the effects were systematically studied. The following conclusions can be drawn from this case study.

(1) A comprehensive geological forecasting system for the watery karst area was established. In this system, TSP is used to detect the fracture of surrounding rocks at a long distance, and GPR and TEM are used to verify the specific location of fracture water at a short distance and mutually. The advanced drilling technology combined with an industrial endoscope can determine the geological conditions ahead more accurately and in less time, and then verify the accuracy of geological forecasting. Finally, the forecasting system detected DK114+70~DK114+95 as a watery karst area

(2) Compared to the displacement of the support structure, curtain grouting thickness is mainly reflected in reducing the amount of water surge. When the grouting thickness exceeds 5 m, the water-stopping effect of the tunnel is almost unchanged. Finally, a grouting thickness of 5 m and a grouting length of 25 m were selected as the grouting range

(3) During grouting, the combination of the three grouting techniques can effectively solve the problems of high water surges and difficult hole formation. The grouting material is mainly sulfoaluminate cement. Cement and cement-sodium silicate were supplemented. The "combination of exploration and injection" method can grasp real-time stratigraphic information and optimize the grouting plan. It is possible to skip holes in areas with good grouting effects and enhance grouting in areas with poor grouting effects

Data Availability

The data that support the findings of this study are available on request from the corresponding author. The data are not publicly available due to privacy or ethical restrictions.

Conflicts of Interest

The authors declare that they have no conflicts of interest.

Acknowledgments

The authors would like to thank the Natural Science Foundation of Hunan Province, grant number 06JJ3030 and the initiation fund for postdoctoral research of Central South University, grant number 228697.

References

[1] B. Liu, Q. Guo, Z. Liu et al., "Comprehensive ahead prospecting for hard rock TBM tunneling in complex limestone geology: a case study in Jilin, China," *Tunnelling and Underground Space Technology*, vol. 93, p. 103045, 2019.

[2] Y. Liu, Y. Feng, M. Xu, Y. Zhang, H. Long, and H. Zhu, "Effect of an incremental change in external water pressure on tunnel lining: a case study from the Tongxi karst tunnel," *Natural Hazards*, vol. 98, no. 2, pp. 343–377, 2019.

[3] Y. Kang, Z. Geng, L. Lu et al., "Compound karst cave treatment and waterproofing strategy for EPB shield tunnelling in karst areas: a case study," *Frontiers in Earth Science*, vol. 9(, 2021.

[4] B. Li, X. Wang, Z. Liu, and T. Li, "Study on multi-field catastrophe evolution laws of water inrush from concealed karst cave in roadway excavation: a case of Jiyuan coal mine," *Geomatics, Natural Hazards and Risk*, vol. 12, no. 1, pp. 222–243, 2021.

[5] X. Huang, Z. H. Xu, and P. Lin, "Identification method of water and mud inrush hazard-causing structures in tunnel and its application," *Journal of Basic Science and Engineering*, vol. 28, no. 1, pp. 103–122, 2020.

[6] A. Alimoradi, A. Moradzadeh, R. Naderi, M. Z. Salehi, and A. Etemadi, "Prediction of geological hazardous zones in front of a tunnel face using TSP-203 and artificial neural networks," *Tunnelling and Underground Space Technology*, vol. 23, no. 6, pp. 711–717, 2008.

[7] M. A. M. Ismail, T. A. Majid, C. O. Goh, S. P. Lim, and C. G. Tan, "Geological assessment for tunnel excavation under river with shallow overburden using surface site investigation data and electrical resistivity tomography," *Measurement*, vol. 144, pp. 260–274, 2019.

[8] S. Li, S. Li, Q. Zhang et al., "Predicting geological hazards during tunnel construction," *Journal of Rock Mechanics and Geotechnical Engineering*, vol. 2, no. 3, pp. 232–242, 2010.

[9] S. Maury, R. K. Tiwari, and S. Balaji, "Joint application of satellite remote sensing, ground penetrating radar (GPR) and resistivity techniques for targeting ground water in fractured ophiolites of South Andaman Island, India," *Environmental Earth Sciences*, vol. 75, no. 3, p. 237, 2016.

[10] E. Slob, M. Sato, and G. Olhoeft, "Surface and borehole ground-penetrating-radar developments," *Geophysics*, vol. 75, no. 5, pp. 75A103–75A120, 2010.

[11] S.-Q. Sun, L.-P. Li, J. Wang, H. Liu, Z. Fang, and X. Ba, "Analysis and prediction of structural plane connectivity in tunnel based on digitalizing image," *KSCE Journal of Civil Engineering*, vol. 23, no. 6, pp. 2679–2689, 2019.

[12] J. A. Doolittle, B. Jenkinson, D. Hopkins, M. Ulmer, and W. Tuttle, "Hydropedological investigations with ground-penetrating radar (GPR): estimating water-table depths and local ground-water flow pattern in areas of coarse-textured soils," *Geoderma*, vol. 131, no. 3-4, pp. 317–329, 2006.

[13] G. Q. Xue, Y. J. Yan, X. Li, and Q. Y. di, "Transient electromagnetic S-inversion in tunnel prediction," *Geophysical Research Letters*, vol. 34, no. 18, 2007.

[14] D. Yang and D. W. Oldenburg, "Three-dimensional inversion of airborne time-domain electromagnetic data with applications to a porphyry deposit," *Geophysics*, vol. 77, no. 2, pp. B23–B34, 2012.

[15] S. C. Li, Z. Q. Zhou, Z. H. Ye, L. P. Li, Q. Q. Zhang, and Z. H. Xu, "Comprehensive geophysical prediction and treatment measures of karst caves in deep buried tunnel," *Journal of Applied Geophysics*, vol. 116, pp. 247–257, 2015.

[16] B. Kravitz, M. Mooney, J. Karlovsek, I. Danielson, and A. Hedayat, "Void detection in two-component annulus grout behind a pre-cast segmental tunnel liner using ground penetrating radar," *Tunnelling and Underground Space Technology*, vol. 83, pp. 381–392, 2019.

[17] D.-Q. Kong, C.-S. Qiao, and G.-C. Xue, "Stability evaluation of flat large-span cavern in jointed rock mass," *Arabian Journal of Geosciences*, vol. 13, no. 11, p. 391, 2020.

[18] G.-H. Zhang, Y.-Y. Jiao, C.-X. Ma, H. Wang, L. B. Chen, and Z. C. Tang, "Alteration characteristics of granite contact zone and treatment measures for inrush hazards during tunnel construction - a case study," *Engineering Geology*, vol. 235, pp. 64–80, 2018.

[19] D. Zhang, Q. Fang, and H. Lou, "Grouting techniques for the unfavorable geological conditions of Xiang'an subsea tunnel in China," *Journal of Rock Mechanics and Geotechnical Engineering*, vol. 6, no. 5, pp. 438–446, 2014.

[20] Y. Maru and T. Maeda, "Construction of the Seikan undersea tunnel–I. General scheme of execution," *Tunnelling and Underground Space Technology*, vol. 1, no. 3-4, pp. 357–371, 1986.

[21] J. Font-Capó, E. Vázquez-Suñé, J. Carrera, D. Martí, R. Carbonell, and A. Pérez-Estaun, "Groundwater inflow prediction in urban tunneling with a tunnel boring machine (TBM)," *Engineering Geology*, vol. 121, no. 1-2, pp. 46–54, 2011.

[22] W. C. Zhu and C. H. Wei, "Numerical simulation on mining-induced water inrushes related to geologic structures using a damage-based hydromechanical model," *Environmental Earth Sciences*, vol. 62, no. 1, pp. 43–54, 2011.

[23] Q. Zhang, P. Li, G. Wang et al., "Parameters optimization of curtain grouting reinforcement cycle in Yonglian tunnel and its application," *Mathematical Problems in Engineering*, vol. 2015, Article ID 615736, 15 pages, 2015.

[24] G. Li, W. Ma, S. Tian, Z. Hongbo, F. Huabin, and W. Zou, "Groundwater inrush control and parameters optimization of curtain grouting reinforcement for the Jingzhai tunnel," *Geofluids*, vol. 2021, Article ID 6634513, 10 pages, 2021.

[25] H. Shi, M. Bai, and S. Xing, "Mechanics parameter optimization and evaluation of curtain grouting material in deep, water-rich karst tunnels," *Advances in Materials Science and Engineering*, vol. 2017, Article ID 1853951, 12 pages, 2017.

[26] J. Liu, W. Chen, J. Yuan, C. Li, Q. Zhang, and X. Li, "Groundwater control and curtain grouting for tunnel construction in completely weathered granite," *Bulletin of Engineering Geology and the Environment*, vol. 77, no. 2, pp. 515–531, 2018.

[27] A. Azimian and R. Ajalloeian, "Permeability and groutability appraisal of the Nargesi dam site in Iran based on the secondary permeability index, joint hydraulic aperture and Lugeon tests," *Bulletin of Engineering Geology and the Environment*, vol. 74, no. 3, pp. 845–859, 2015.

[28] J.-Q. Liu, W.-Z. Chen, K.-V. Yuen, and X. S. Zhou, "Groundwater-mud control and safety thickness of curtain grouting for the Junchang tunnel: a case study," *Tunnelling and Underground Space Technology*, vol. 103, p. 103429, 2020.

[29] J. Yuan, W. Chen, X. Tan, D. Yang, and S. Wang, "Countermeasures of water and mud inrush disaster in completely weathered granite tunnels: a case study," *Environmental Earth Sciences*, vol. 78, no. 18, p. 576, 2019.

[30] J. Niu, Y. Sun, B. Wang et al., "Grouting treatment of water and mud inrush in fully weathered granite tunnel: a case study," *Geofluids*, vol. 2020, Article ID 8838769, 18 pages, 2020.

[31] The Second Railway Survey and Design Institute, *Code for Design on Tunnel of Railway (in China)*, Trade Standards-Railway, 2005, A5.

[32] Specification for grouting (in China) YSJ. 211-1992.

[33] X. Y. Wang, M. S. Wang, and M. Zhang, "Research on regulating water pressure acting on mountain tunnels by blocking ground water and limiting discharge," *Chinese Journal of Geotechnical Engineering*, vol. 1, pp. 125–127, 2005.